Original Research

Fabrication, Characterization, and Simulation of Paraffin/ Kaolin/ Carbon Nanotube Composite Phase Change Materials for Shell-and-Tube Thermal Energy Storage Unit

Tieying Wang [1,*], Yuanxiang Su [1], Songsong Liu [1], Shuai Ma [1], Qiaolong Zhang [1], Binjie Yao [1], Xinxin Guang [1]

[1] Tianjin Key Laboratory of Refrigeration Technology, Tianjin University of Commerce, Tianjin 300134, China
* Correspondence: wangtieying@tjcu.edu.cn

Received: February 11, 2026; Accepted: June 12, 2026

Abstract: In this work, shape-stabilized composite phase change materials (SSPCMs) were fabricated using paraffin (PA) as the phase change medium, kaolin as the supporting framework, and multi-walled carbon nanotubes (MWCNT) as thermal conductivity enhancers. Five SSPCMs specimens with MWCNT mass fractions of 0%, 2.5%, 5%, 7.5% and 10% were prepared at a constant kaolin-to-PA mass ratio of 3:7. The microstructure, chemical compatibility, thermal conductivity, specific heat capacity and latent heat were comprehensively characterized. The layered and porous structure of kaolin and MWCNT enabled favorable encapsulation of PA, and only physical interactions occurred among components, guaranteeing superior chemical stability. With the increase of MWCNT content, the specific heat capacity and latent heat gradually decreased, whereas thermal conductivity exhibited a monotonic increase. The SSPCM with 10% MWCNT possessed a thermal conductivity of 1.88 W/m·K, which was 5 times higher than that of pure PA. Numerical investigation on a finned latent heat thermal energy storage (LHTES) device indicated that MWCNT incorporation effectively reduced thermal energy storage duration and elevated energy storage efficiency.

Keywords: thermal energy storage; paraffin; carbon nanotubes; kaolin; energy storage efficiency

1. Introduction

Thermal energy is widely present in human daily life. For example, cars burn gasoline to generate heat, food is cooked by heating, and electric heating is used for warmth, etc. If used improperly, it can easily generate a large amount of waste heat [1]. Therefore, how to efficiently and reasonably utilize and storage heat energy has become an important research topic in the current energy field [2-4].

Thermal energy storage (TES) technology is one of the effective means to achieve highly efficient utilization of thermal energy. TES mainly includes three forms: sensible heat storage, thermochemical storage, and latent heat storage [5, 6]. Among them, latent heat thermal energy storage (LHTES) plays an increasingly important role in alleviating the contradiction between energy supply and demand and improving the efficiency of the energy system due to its advantages such as high energy storage density, small temperature fluctuation during storage, and high technical maturity. It has been widely applied in solar thermal power generation, building energy conservation, and other fields [7-9].

The core of this technology lies in the phase change materials (PCMs). PCM can absorb or release a large amount of latent heat at a relatively constant temperature during the phase change process, thereby achieving efficient energy storage and release [10].

Paraffin wax(PA), as a commonly used organic phase change material, possesses high latent heat storage capacity, is non-toxic and non-corrosive, and has good chemical stability [11]. However, phase change materials such as PA generally have a low thermal conductivity, and they are prone to leakage in practical applications, thereby reducing the charging and discharging efficiency of the system [12]. To address these issues, high thermal conductivity porous materials are usually used as the supporting matrix to prepare stable phase change materials. Such materials can not only effectively prevent the leakage of phase change materials but also significantly improve their thermal conductivity [13-15].

Currently, the commonly used base materials mainly include inorganic materials [16, 17], polymer foams [18], activated carbon [19, 20], and metal structures [21, 22], etc. The structural integrity and cost-effectiveness of the base material are also key factors to be considered during the selection process [23]. During actual operation, metal-based PCM still have potential problems such as leakage, corrosion, and high cost [24]. In contrast, carbon-based porous materials, due to their high specific surface area, excellent thermal conductivity, and multi-scale pore structure, become ideal supporting matrices for phase change materials, helping to enhance their adsorption and encapsulation performance. Moreover, these materials also possess good high-temperature resistance, hydrophobicity, acid and alkali resistance, and thermal response capabilities, demonstrating excellent comprehensive thermal management performance [25].

To further enhance the latent heat storage performance and expand the application potential of shape-stabilized composite phase change materials (SSPCMs), Cao et al. [26] prepared ultra-high molecular weight polyethylene (UHMWPE)/carbon nanotube (CNT) composite porous frameworks using microwave sintering technology, and introduced PA into the framework through vacuum impregnation. They successfully prepared SSPCMs. Experimental results showed that the leakage rate of this material was only 2.3% when it operated at 70°C for a long time, demonstrating excellent stability. Kanti et al. [27] prepared MWCNT–Al_2O_3 hybrid nanoparticle-reinforced paraffin-based phase change materials. The thermal properties under different hybrid ratios and filler contents were investigated, and two prediction models namely XGBoost and SMO were established. The experimental results show that the thermal conductivity is increased by 36.1% at a filler content of 2 wt% and a hybrid ratio of 80:20. At the dosage of 1 wt%, the optimal enhancement of crystallization latent heat and melting latent heat is achieved at the ratios of 20:80 and 80:20, respectively. Thermogravimetric analysis confirms the good thermal stability of the materials. In addition, XGBoost presents obviously higher prediction accuracy than SMO, which can effectively predict the thermal conductivity and latent heat properties.

Ren et al. [28] studied a method of loading PA through gas-phase deposition onto the composite structure of CNT and expanded perlite, effectively inhibiting the leakage of PA and increasing the thermal conductivity of the material by 2.96 times. Karaipekli et al. [29] used CNT as the supporting material to prepare and characterize the expanded perlite/n-pentadecane (C20) composite material, and evaluated its TES performance as a new form-stable composite phase change material . It was found that when ExP was loaded with 60 wt% C20, no leakage occurred.

Subasi et al. [30] prepared a series of unsaturated polyester resin /CNT/microcapsule phase change material composite systems by combining mechanical mixing and ultrasonic treatment, and post-treated the materials using UV curing technology. Temperature test results showed that the introduction of MPCM significantly enhanced the TES capacity of the composite material. Lv et al. [31] used vacuum impregnation to combine different particle sizes of kaolin with PA, and the resulting material exhibited good thermal stability.

However, there are still certain limitations in the current research on the CNT and kaolin composite system in improving thermal conductivity and structural stability, and further optimization and exploration are still needed.

From the perspectives of economy and environmental friendliness, it is urgent to develop a matrix material with high thermal conductivity, high stability and environmental friendliness for loading PA. Moreover, existing studies mainly focus on the preparation and characterization of PA-based shape-stabilized phase change materials, while there is relatively less research on their practical application in latent heat storage devices. Further exploration is still needed to verify their feasibility in engineering practice.

To address the aforementioned issues, this paper developed a novel shape-stabilized composite phase change material based on PA as the PCM, and kaolin and MWCNT the supporting matrix. The microstructure, chemical compatibility, thermal conductivity, latent heat of phase change, and cycling stability of this material are systematically analyzed. Furthermore, the prepared SSPCMs are applied in latent heat storage devices for numerical simulation studies, and integrated into a vertical shell-and-tube latent heat storage device to deeply explore their heat transfer performance and energy storage behavior.

2. Experiment section

2.1. Raw materials

The PA (powder form, 300 mesh, the phase transition temperature is shown in Figure 1.) used in this research was purchased from Kaixuan Plastic Technology Co., Ltd. in Dongguan City, Guangdong Province, China; kaolin was provided by Aladdin Biochemical Technology Co., Ltd. in Shanghai, China; and MWCNT were procured from Changzhou Carbonbo New Materials Technology Co., Ltd.

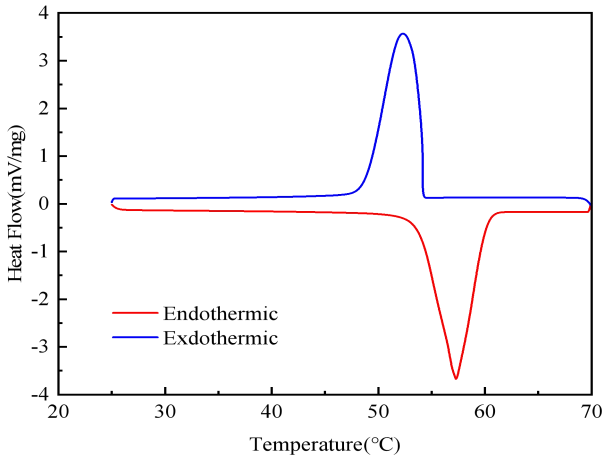

Figure 1. DSC curves of PA for the melting and the freezing process.

2.2. Fabrication of PA/kaolin/MWCNT SSPCMs

In this study, PA was selected as the phase change material, and kaolin and MWCNT were used as the matrix materials to prepare the shaped phase change heat storage material. The material preparation process is shown in Figure 2. Preliminary experimental results indicate that a kaolin-to-PA mass ratio of 3:7 yields the optimal trade-off between morphological stability and total energy storage capacity. Therefore the mass ratio of kaolin to PA was fixed at 3:7. First, according to the five different ratios shown in Table 1, PA, kaolin and MWCNT were accurately weighed using an electronic balance with a precision of 0.1 mg and placed on clean weighing paper. Then, the mixed materials were transferred into a centrifuge tube and blended uniformly on a digital constant-speed mixer at a rotational speed of 100 r/min for 2 hours to ensure full dispersion of the components. The five groups of uniformly mixed sample powders were then transferred into standard

circular molds with a diameter of 5 mm, and compressed on a precision press machine under a pressure of 5 MPa for 3 minutes to maintain stable molding pressure and obtain uniform disc-shaped samples. After cold pressing, the samples were placed in a programmable constant-temperature furnace for sintering treatment. The temperature was raised from room temperature to 80 ℃ at a steady heating rate of 5 ℃/min, and held isothermally at 80 ℃ for 16 minutes to ensure sufficient infiltration and shaping. Finally, the samples were naturally cooled to room temperature inside the furnace to avoid thermal shock, and five labeled samples: SSPCM-1, SSPCM-2, SSPCM-3, SSPCM-4 and SSPCM-5 were obtained. Mechanical stirring was adopted to homogenize the composite materials in this work. The subsequent results indicate that this method can meet the experimental requirements, while it still exhibits inherent limitations. Accordingly, ultrasonic dispersion is recommended for the homogenization treatment of composite materials [32].

Table 1. Compositions of the SSPCMs.

Samples	SSPCM-1	SSPCM-2	SSPCM-3	SSPCM-4	SSPCM-5
PA(wt.%)	70	68.25	66.5	64.75	63
Kaolin(wt.%)	30	29.25	28.5	27.75	27
MWCNT(wt.%)	0	2.5	5	7.5	10

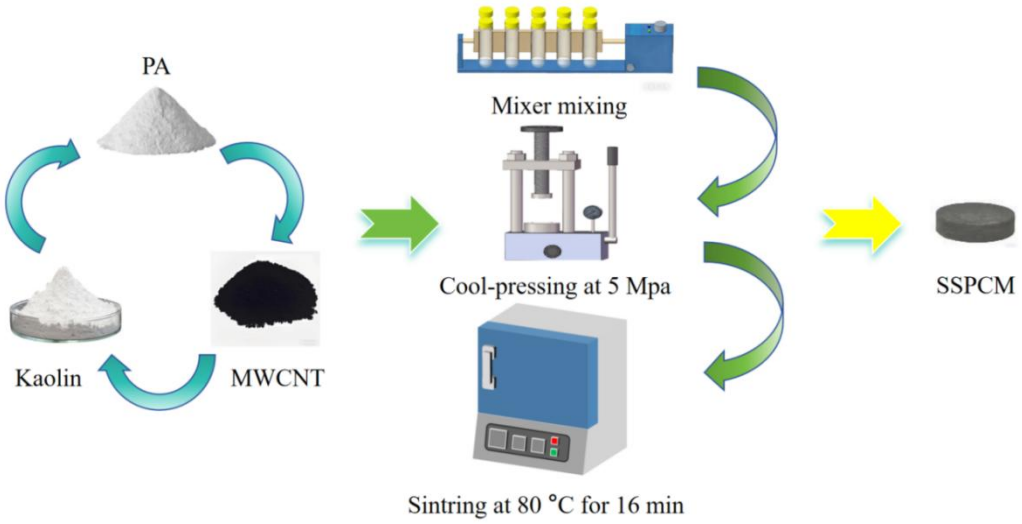

Figure 2. Flow chart of SSPCMs preparation.

2.3. Characterization

After the sample preparation was completed, leakage performance tests were conducted on SSPCM-1~SSPCM-5. The microstructure of the composite materials was characterized using a field emission scanning electron microscope (SEM, Thermo Scientific Apreo 2C, USA) at an accelerating voltage of 10 kV. To enhance the conductivity of the samples, P_t spraying treatment was performed on the surface of the samples before observation. The chemical structures of PA, kaolin, MWCNT, and SSPCMs were analyzed and identified using a Fourier transform infrared spectrometer (FT-IR, Spectrum Two, PerkinElmer, USA), with the test wave number range being 450 - 4000 cm^{-1}. The phase transformation characteristics of the samples were determined using differential scanning calorimetry (DSC, TAG 20, USA) in a nitrogen (N_2) atmosphere, with a heating rate of 3 ℃/min and a test temperature range of 25 - 70 ℃. The thermal conductivity of the

samples was measured using a thermal constant analyzer (Hot Disk, 2500S, Sweden).

3. Results and discussion

3.1. Leakage experiments

To assess whether the five phase-change materials prepared have any leakage phenomenon, this study conducted a leakage performance test on them. The specific operation was as follows: The prepared SSPCMs samples were placed in a muffle furnace and heated at a rate of 5 ℃/min from room temperature to 80 ℃, and then kept at this temperature for 30 minutes. At the same time, the mass of the samples before and after heating was weighed separately to analyze their thermal stability and leakage behavior.

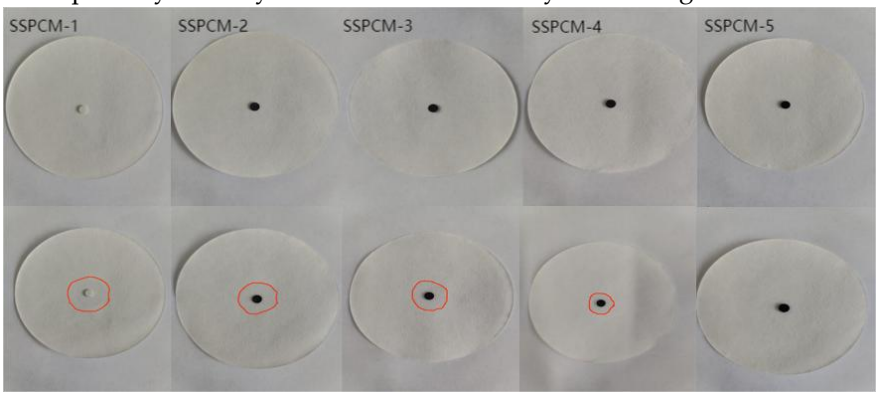

Figure 3. Leakage diagrams of five composite phase change materials before sintering and after sintering and holding at temperature for 30 minutes.

As shown in Figure 3, the upper part of the figure presents the microscopic morphology of SSPCM-1~SSPCM-5 in the un-sintered state, while the lower part shows their leakage conditions after sintering and being held at 80℃ for 30 minutes. According to the leakage test results, SSPCM-1~SSPCM-5 can maintain a relatively stable geometric structure before and after heating. Among them, SSPCM-1~SSPCM-3 show a relatively obvious leakage phenomenon, SSPCM-4 has a slightly lighter leakage degree, and SSPCM-5 hardly shows any leakage. By comparing the volume and mass changes of the samples before and after the experiment, it can be found that the volume of SSPCM-1 decreased by 29.1%, SSPCM-2 a 22.3% reduction, SSPCM-3 an 18.8% reduction, SSPCM-4 an 11.6% reduction and the volume of SSPCM-5 decreased by 4.7%. In terms of mass, SSPCM-1 decreased by 33.4%, SSPCM-2 decreased by 30.5%, SSPCM-3 decreased by 25.1%, SSPCM-4 decreased by 15.3% and SSPCM-5 decreased by 3.4%. The leakage test results demonstrate that despite the relatively high degree of PA leakage observed in SSPCM-1 and SSPCM-2, all five composite phase change materials are capable of maintaining excellent shape stability, so the subsequent performance characterization and structural analysis will be further carried out based on these five samples.

3.2. Microscopic structure analysis

Figure 4a shows the microscopic morphology of PA under an electron microscope, presenting a uniform and dense structural feature. The particles are distributed in an irregular block-like pattern. The surface has obvious concavities, fissures and texture features, allowing for clear observation of individual particles and their boundaries. Figure 4b shows that kaolin has a typical sheet-like structure, with well-developed pore structures between the layers, giving it excellent adsorption capacity, which helps to effectively inhibit the leakage behavior during the solid-liquid phase transition of PA. Figure 4c shows that MWCNT present a tubular-like structure. Their surface is

composed of interwoven and interlaced network structures, and the overall surface morphology is clearly visible, including fine surface textures and tubular channels.

Figure 4d to 4h show the microstructure characteristics of SSPCM-1~SSPCM-5. It can be observed that there are certain gaps between the kaolin layers, and the PA is tightly adsorbed between their layered structures. Due to its abundant fibrous structure, MWCNT are easy to intertwine and interweave with each other. When combined with PA, their intertwined structure can effectively encapsulate the PA molecules. As the content of the matrix increases, the overall structure of SSPCMs tends to become more dense. The matrix builds a continuous three-dimensional thermal conduction network through its layered and fibrous structures, providing an efficient heat transfer path and significantly enhancing the thermal stability of the material. MWCNT play the role of a bridge between PA and layered kaolin, closely binding the components together, thereby forming an efficient three-dimensional heat transfer channel. From the SEM images (Figure 4d–h), no severe agglomeration of MWCNT is observed in all samples. MWCNT are uniformly dispersed in the kaolin/paraffin matrix and interweave with each other to form a continuous three-dimensional thermal network. Only slight local entanglement appears at 10 wt% MWCNT, without forming compact agglomerate bundles. The good dispersion ensures the steady linear increase of thermal conductivity with MWCNT content (Figure 8), and no performance stagnation caused by agglomeration is found. Meanwhile, the uniform dispersion guarantees excellent homogeneity and experimental reproducibility.

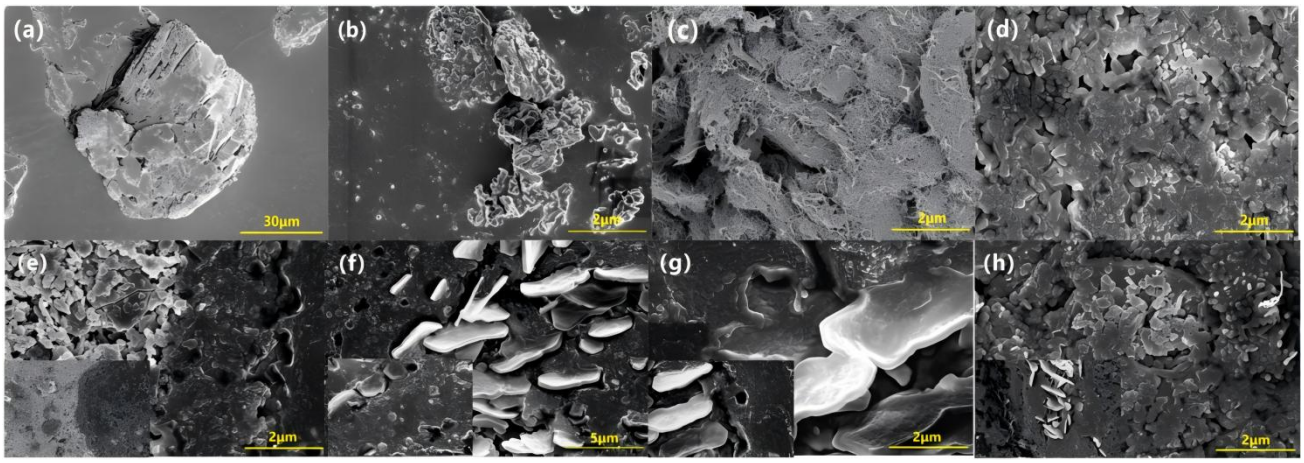

Figure 4. SEM photos of (a) PA (b) kaolin (c) MWCNT (d) SSPCM-1 (e) SSPCM-2 (f) SSPCM-3 (g) SSPCM-4 (h) SSPCM-5.

3.3. Chemical compatibility analysis

The chemical compatibility between PA and kaolin is of great significance for the performance of the composite material. Fig. 5 shows the FT-IR spectra of PA, kaolin, MWCNT, and SSPCM-1~SSPCM-5 within the wavenumber range of 450 - 4000 cm^{-1}. From Figure 5 , it can be seen that the infrared spectrum of PA shows typical absorption peaks at 721 cm^{-1}, 935 cm^{-1}, 1295 cm^{-1}, 1693 cm^{-1}, 2848 cm^{-1}, and 2914 cm^{-1}, which correspond to the rocking vibration peaks of $-CH_2$ groups, the bending vibration peaks of $-CH_2$ and $-CH_3$ groups, and the stretching vibration peaks of $-CH_2$ and $-CH_3$ groups [33]. The infrared spectrum of kaolin shows two characteristic absorption peaks at 834 cm^{-1} and 1099 cm^{-1}, corresponding to the bending vibration peak of Al-OH and the broad stretching vibration peak of Si-O-Si [34]. The spectrum of MWCNT shows a characteristic peak at 2735 $cm^{-1,}$ attributed to the stretching vibration of C-H bond [35]. In the infrared spectra of SSPCM-1~SSPCM-5, only the characteristic absorption peaks of PA, kaolin, and MWCNT are observed, and no new chemical bonds are detected. Thus, the synthesis process of this type of stable phase-change material

belongs to a physical mixture process and no chemical reaction occurs.

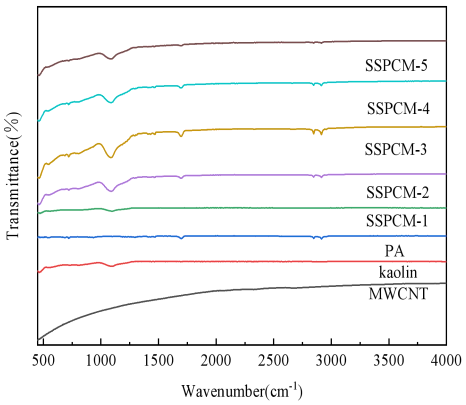

Figure 5. FT-IR patterns of PA, kaolin, MWCNT, SSPCM-1, SSPCM-2, SSPCM-3, SSPCM-4, and SSPCM-5.

3.4. Phase change process of SSPCMs

DSC is an important analytical method used to determine the heat storage capacity and phase transition temperatures of materials. Figure 6 shows the DSC heat absorption and release curves of PA and the phase change materials formed by combining PA with five different matrix ratios. Table 2 further summarizes the key parameters reflecting the phase transition process in the DSC curves.

The DSC analysis results indicate that the DSC curves of SSPCMs and pure PA are highly similar. The melting point of pure PA is 54.18℃. The melting points of SSPCM-1 to SSPCM-5 are 53.72 ℃, 53.7 ℃, 53.8 ℃, 53.81 ℃ and 53.86 ℃, respectively, which are slightly lower than that of pure PA, It might be that the addition of the matrix weakened the intermolecular forces of the PA, making it easier for the PA molecules to break away from the crystal structure, and thus the melting point decreased slightly [36]. Indicating that the introduction of the matrix has a slight impact on the melting point.

During the melting and solidification processes, SSPCMs shows only one phase transition peak, which is consistent with that of pure PA. In addition, the peak temperatures of heat absorption and release of pure PA are higher than those of SSPCMs, which may be attributed to the hindrance effect of the matrix material on heat conduction, thereby affecting the kinetic behavior of the phase transition process [37]. The phase transition behavior during the heat absorption process, as one of the key parameters, is an important basis for evaluating the heat storage performance of SSPCMs.

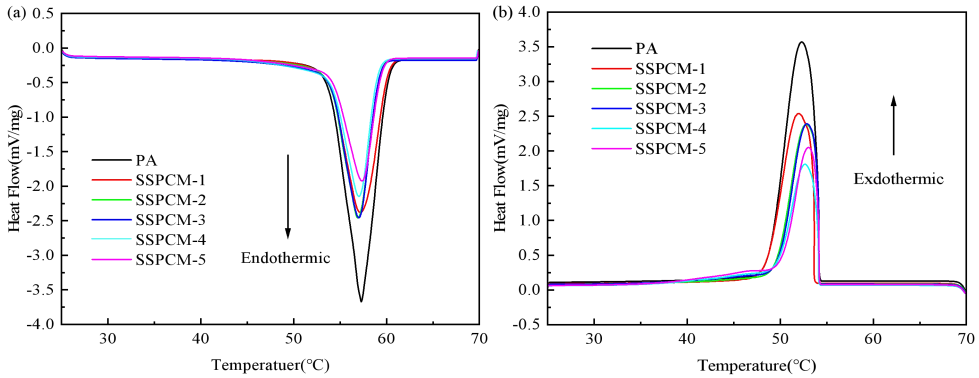

Figure 6. DSC curves of PA, SSPCMs for the (a) melting and the (b) freezing process.

Table 2. Phase transition results for PA and SSPCMs.

Samples	Start-temperature Ts (◦C) Melting/Freezing process	End-temperature Te (◦C) Melting/Freezing process	Latent heat ΔH(J/ g) Melting/ Freezing Process
PA	54.18/54.17	60.21/48.79	253.2/248.1
SSPCM-1	53.72/53.72	60.17/48.5	174.6/174
SSPCM-2	53.7/54.19	59.32/49.63	166.1/165.5
SSPCM-3	53.8/53.81	59.29/52.86	162.7/160.6
SSPCM-4	53.81/54.11	59.49/49.82	159.1/157.5
SSPCM-5	53.86/54.18	59.2/50.34	154/152.6

As shown in Table 2, the latent heat of phase transition of SSPCMs is lower than that of pure PA. This is mainly due to the fact that kaolin and MWCNT did not undergo phase transition during the process of absorbing and releasing heat, while only PA in SSPCMs underwent phase transition. Moreover, as the content of the matrix increases, the mass proportion of the PCM decreases accordingly, resulting in a decrease in the overall latent heat of phase transition of SSPCMs. To evaluate the difference between the experimental values and theoretical values of SSPCMs, the following calculation formula is used for comparison:

$$\Delta H = \eta \Delta H_{PCM} \tag{1}$$

where ΔH represents the latent heat of phase transition of SSPCMs, η represents the mass fraction of the phase change material in SSPCMs, and ΔH_{PCM} is the melting enthalpy value of PA. Figure 7 shows the experimental measured values and theoretical calculated values of SSPCMs. It can be seen that the measured heat absorption of SSPCMs is slightly lower than the theoretical value, it is possible that the arrangement of the PA molecules around the substrate has changed, thereby altering the local steric hindrance [38]. Overall, the actual heat storage performance of SSPCMs is close to the theoretical expectation and possesses good thermal energy storage capacity.

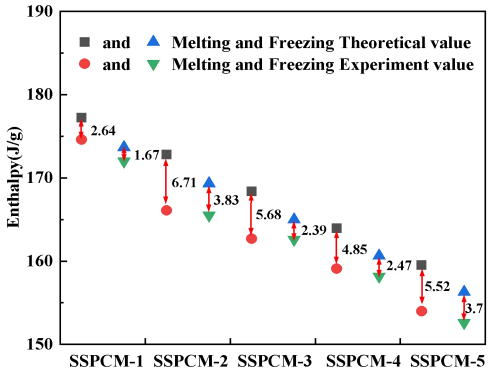

Figure 7. Comparison of the measured and theoretical enthalpies for the SSPCMs.

3.5. Thermal performance of SSPCMs

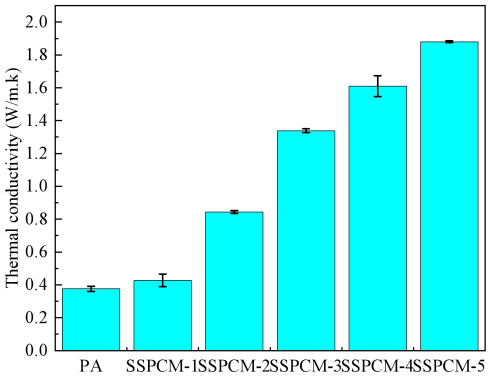

Figure 8. Thermal conductivity of PA and SSPCMs with different kaolin and MWCNT contents.

In addition to the heating and melting temperatures, the thermal conductivity of energy storage materials is also an important factor for evaluating energy storage performance. Since the main heat transfer mode of SSPCMs is conduction, the high thermal conductivity of SSPCMs can complete the energy storage and release processes more quickly and store more energy. PA has a high potential thermal performance, but its thermal conductivity is relatively low, typically ranging from 0.2-0.4 W/(m·K). The thermal conductivity of SSPCMs was measured using a thermal constant analyzer. Figure 8 shows the thermal conductivities of PA and SSPCMs. The thermal conductivities of PA, SSPCM-1, SSPCM-2, SSPCM-3, SSPCM-4 and SSPCM-5 are 0.3759 W/(m·K), 0.4272 W/(m·K), 0.8438 W/(m·K), 1.3385 W/(m·K), 1.6105 W/(m·K) and 1.88 W/(m·K), respectively. The thermal conductivity increases gradually, indicating that no obvious agglomeration of MWCNT occurs in the composite, which is consistent with the microstructure analysis of the composite in Figure 4.The predicted thermal conductivity of SSPCM-5 is capable of reaching 2 W/m·K. This deviation between the predicted and measured values is presumably ascribed to the partial agglomeration of multi-walled MWCNT induced by the increased MWCNT content, which further results in a relatively lower thermal conductivity in practical measurements. Minor numerical discrepancies are observed in the measured thermal conductivity of SSPCMs. Such discrepancies are presumably ascribed to the measurement being conducted in an open atmospheric environment, where no thermal insulation treatment was applied to the surface of the composite samples. It is therefore recommended that subsequent measurements be carried out under isothermal conditions to guarantee the stability and accuracy of the test results. Recent studies showed that single addition of MWCNT in stearic acid could only increase thermal conductivity to about 0.83 W/m·K [39]. In this work, the thermal conductivity of SSPCM-5 is 5 times that of PA. This is because MWCNT have higher thermal conductivity than PA, forming better heat transfer channels and networks in SSPCMs. Moreover, as the content of the matrix skeleton increases, the thermal conductivity of SSPCMs also increases.

In the experiment, sapphire was used as the reference material, and the specific heat capacity (CP) of the material in the solid and liquid states was measured by the differential scanning calorimeter. According to Figure 9, regardless of whether it is in the solid state or the liquid state, Cp shows slight fluctuations with temperature, and shows more significant changes near the phase transition region. Table 3 presents the equation derived from fitting the Cp curve using Origin software, demonstrating a quadratic functional relationship between temperature and specific heat capacity.

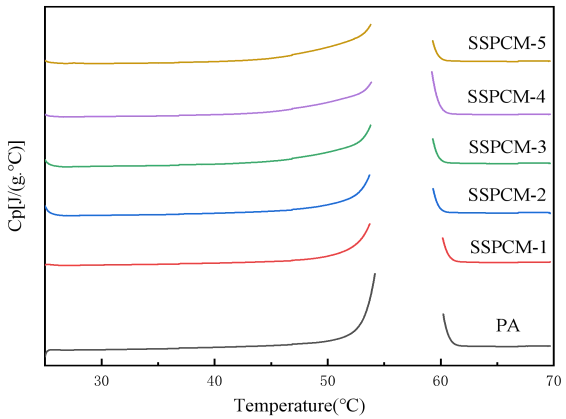

Figure 9. Specific heat capacity of PA and SSPCMs before and after phase change.

Table 3. Correlation of specific heat capacity of PA and SSPCMs.

Sample	States	Cp(J/g·℃)
PA	Solid	53252.74881-53250.77378/(1+exp.((T-67.08659)/1.45386))
	Liquid	2.14359+11.23725/(1+exp.((T-59.95514)/0.34364))
SSPCM-1	Solid	23135.71026-23133.85184/(1+exp.((T-76.01127)/2.56263))
	Liquid	2.05302+10.87213/(1+exp.((T-59.76714)/0.36758))
SSPCM-2	Solid	22070.5819-22068.65784/(1+exp.((T-81.20826)/3.14839))
	Liquid	2.08398+10.18501/(1+exp.((T-58.98687)/0.32892))
SSPCM-3	Solid	11653.19366-11651.25966/(1+exp.((T-89.11308)/4.37843))
	Liquid	2.21737+12.87958/(1+exp.((T-58.84635)/0.34323))
SSPCM-4	Solid	1969.41382-1967.84514/(1+exp.((T-86.17167)/5.06777))
	Liquid	1.81509+12.63668/(1+exp.((T-59.01689)/0.3787))
SSPCM-5	Solid	1383.08467-1381.31003/(1+exp.((T-81.71431)/4.76116))
	Liquid	2.01851+12.94222/(1+exp.((T-58.73537)/0.3593))

Figure 10 shows the energy storage density of PA and SSPCM-1~SSPCM-5. Within the temperature range of 25 to 70 ℃, the energy storage density can be calculated and represented by Equation (2):

$$Q = \int_{25}^{T_s} C_s dT + \Delta H + \int_{T_e}^{70} C_l dT \quad (2)$$

where C_S represents the solid-state specific heat capacity of SSPCMs, C_l is the liquid-state specific heat capacity of SSPCMs, T_s is the temperature at which the phase transition begins, T_e is the temperature at which the phase transition ends. ΔH is the latent heat of phase transition of SSPCMs.

As shown in Figure 10, the energy storage density of the composite material gradually decreases with the increase in the content of the matrix (SSPCM-1 (258.3 J/g) > SSPCM-2 (248.4 J/g) > SSPCM-3 (242.4 J/g) > SSPCM-4 (235.6 J/g) > SSPCM-5 (226.4 J/g)). This phenomenon can be attributed to the decrease in the latent heat of phase transition of the composite material due to the increase in the content of the matrix (Table 2). Since the specific heat capacity of kaolin and MWCNT is lower than that of PA, and the latent heat of the composite material is entirely derived from PA, when the content of the matrix increases, the proportion of PA decreases relatively, thereby causing the energy storage density of SSPCM to decrease accordingly.

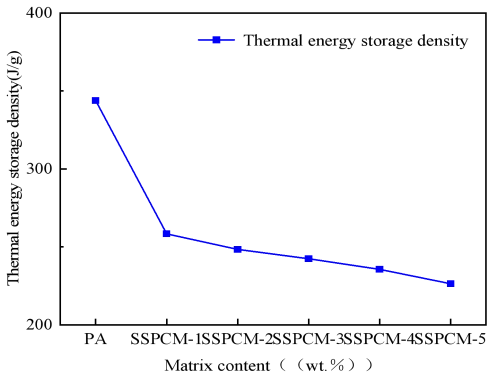

Figure 10. Thermal energy storage densities of composites as a function of PA and SSPCMs.

3.6. Potential application in thermal energy storage device

3.6.1 Physical model and computational domain

As shown in Figure 11(a), this study designed a vertical shell-and-tube LHTES device unit. This LHTES unit is mainly composed of two concentric cylinders, with a total length of 400 mm. The inner layer is a stainless steel tube with a diameter of 15 mm and a wall thickness of 2.5 mm; the outer layer is an acrylic shell with a diameter of 44 mm. On the outer surface of the stainless steel tube, 56 ring-shaped fins with a height of 10 mm and a thickness of 0.257 mm are uniformly arranged. The heat transfer fluid (HTF) is water, which is injected from the top, and the inlet temperature is set at 80℃. The flow velocity of the heat fluid is constant at 0.01 m/s, which is based on the research results of Longeon et al., aiming to ensure effective heat transfer for a long time in the shell-and-tube heat exchanger (based on the Reynolds number calculated from the pipe diameter, it is lower than 2300), thereby ensuring that the fluid is in a laminar state within the pipe. The initial temperatures of the SSPCMs and the LHTES device are uniformly set at 25℃. After the heat fluid is injected into the system, continuous convective heat transfer occurs between the HTF and the solid phase change material, with heat being conducted through the ring-shaped fins to the composite material and ultimately stored in the SSPCMs. Considering that the model has axisymmetric characteristics, to reduce computational resource consumption, the model is simplified to half of the two-dimensional computational domain, as shown in Figure 11(b). At the same time, five monitoring points along the axial direction are selected for temperature collection, ensuring that these points are not located in the fin area, so as to facilitate the subsequent calculation and analysis of the liquid phase ratio(Figure 11(c)). The five points are 10mm away from the outer surface of the stainless steel. P3 is at the center, P1 is 150mm away from the center, P2 is 75mm away from the center, P4 is symmetrical to P2, and P5 is symmetrical to P1.

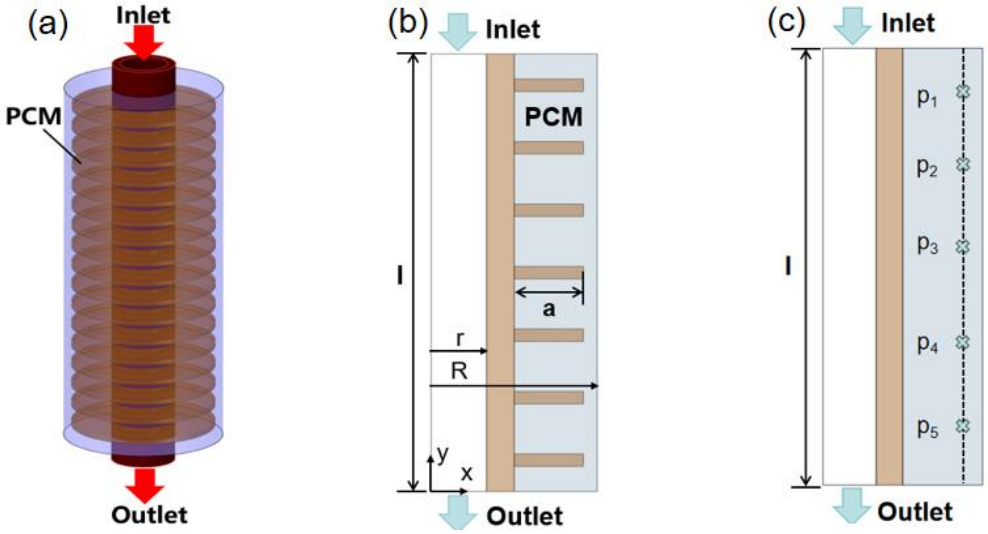

Figure 11. (a) Schematic of the shell-and-tube LHTES unit with annular fins; (b) computational domain;(c) Sampling points.

3.6.2 Control equations and boundary conditions

During the heat transfer process of composite materials, the main heat transfer mechanism is heat conduction. To facilitate model analysis, the following assumptions are proposed in this paper:

(1) SSPCMs have continuity, isotropy and homogeneity;

(2) Due to the stability of the material structure, the volume changes that occur during the phase transition can be ignored

For the outer surface, although the thermal conductivity of plexiglass is relatively low (0.2 W/m·K), there is still inevitable heat loss. This heat loss is mainly transferred through natural convection between the outer surface of the plexiglass and the surrounding air. The natural convection heat transfer process can be estimated using the following empirical formula [40]:

$$Q = hA(T_w - T_e) \tag{3}$$

where A represents the surface area of the organic glass, T_W and T_e are the temperatures of the organic glass surface and the ambient air respectively, and h is the natural convection heat transfer coefficient, which is estimated through empirical correlation formulas:

$$h = \frac{0.59k}{D}(GrPr)^{\frac{1}{4}} \tag{4}$$

where k represents the thermal conductivity of air, and D is the characteristic dimension.

Based on the above assumptions, the phase change process of the composite materials in the thermal energy storage device was analyzed, and the governing equations are as follows.

For HTF: The fluid flow and convective heat transfer are determined by the following equations:

$$\nabla \cdot \vec{u} = 0 \tag{5}$$

$$\rho_{HTF}\frac{\partial u}{\partial t} + \rho_{HTF}(\vec{u}\cdot\nabla)\vec{u} = -\nabla P + \mu_{HTF}\nabla^2\vec{u} \tag{6}$$

$$\rho_{HTF}C_{p_{HTF}}\frac{\partial T}{\partial t} + \rho_{HTF}C_{p_{HTF}}\vec{u}\cdot\nabla T = \nabla\cdot(k_{HTF}\nabla T) \tag{7}$$

For PCM, the energy equation is:

$$\frac{\partial(\rho_s H)}{\partial t} = \nabla \cdot (k_s \nabla T_s) \tag{8}$$

where ρ_{HTF},C_{pHTF} and k_{HTF} represent the density, specific heat and thermal conductivity of HTF, respectively, while T represents the temperature of HTF; ρ_s, k_s and T_s represent the density, thermal conductivity and temperature of the composite material, respectively, and t represents time. H is the total enthalpy of the composite material, which is composed of finite enthalpy (h) and latent heat enthalpy (Δh).

$$H = h + \Delta h \tag{9}$$

$$h = h_{ref} + \int_{T_{ref}}^{T} C_s dT \tag{10}$$

$$\Delta h = \beta L \tag{11}$$

$$\beta = \begin{cases} 0 & if\ T_{PCM} < T_s \\ \dfrac{T_{PCM} - T_s}{T_l - T_s} & if\ T_s \le TPCM \le T_l \\ 1 & if\ T_{PCM} > T_l \end{cases} \tag{12}$$

where h_{ref} ,T_{ref} , and C_s represented the reference enthalpy, reference temperature, and specific heat of composite SSPCMs, respectively. L denoted the latent heat of SSPCMs, and β denoted the liquid fraction ranging from 0 to 1. TPCM , T_l , and T_s was the temperature, melting temperature, and solidification temperature of PCMs, respectively.

Based on the above assumptions and the simplified computational domain, this study uses the commercial software ANSYS-Fluent based on the finite volume method (FVM) to solve the governing equations for the problems involving moving boundaries and transient heat transfer. The initial temperatures of the HTF, PCM, and heat transfer tubes are all 25 ℃. Hot water with a temperature of 80 ℃ and a flow rate of 0.01 m/s flows from the top inlet, and the left wall of the computational domain is set as an axisymmetric boundary. The pressure and velocity coupling uses the semi-implicit pressure-velocity coupling algorithm (SIMPLE), the spatial discretization of the pressure term adopts the PRESTO! format to improve numerical accuracy and avoid interpolation errors at the boundaries and the standard discretization assumption for pressure gradients; the momentum equation and energy equation are discretized spatially using the second-order upwind scheme. The convergence criteria for the continuity equation, momentum equation, and energy equation are set as 10-3, 10-3, and 10-6 respectively. The inlet boundary condition is set as a velocity inlet, and the outlet boundary condition is set as a pressure outlet.

To eliminate the influence of mesh quantity on the phase change process, a mesh independence verification was carried out.Four different mesh numbers were adopted for the verification, namely 18462, 59282, 222038 and 392048.Table 4 presents the liquid fraction, HTF outlet temperature at 1000 s, and the complete melting time under different mesh quantities and time steps. To ensure the calculation accuracy while also considering the computational efficiency, the final determined number of meshes is 221,087, and the time step is 0.1 s. To verify the reliability of the numerical model, the simulation results are compared with those in reference [41], as shown in Figure 12. The results show that the temperature change trend during charging is basically the same, and the maximum error is less than 4.3%. Therefore, the numerical model adopted in this study has a high degree of credibility.

Table 4. Verification of grid size and time step.

Mesh number	Time step (s)	Melting time (s)	Outlet temperature(℃)	Liquid fraction
59282	0.5	6325	48.3	0.382
184624	0.5	6407	50	0.371
222038	0.5	6489	50.2	0.364
392048	0.5	6523	50.3	0.36
222038	0.1	6521	50.5	0.362
222038	0.05	6539	50.5	0.36

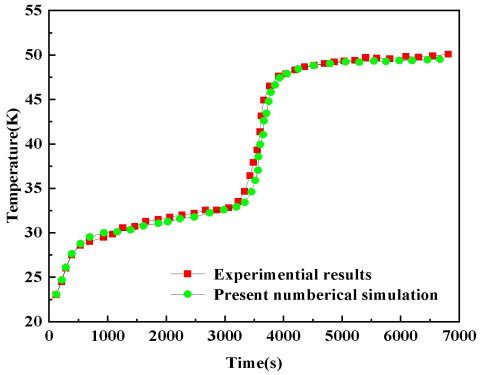

Figure 12. Comparison with the experimental results in the literature [41].

3.6.3 Charging and discharging performance

To quantitatively analyze the temperature evolution characteristics of SSPCMs during the charging process, Figure 13 shows the temperature change process at the selected monitoring points in the radial direction. The temperature change trends of the five materials at different points are basically the same. Taking SSPCM-1 and SSPCM-5 as examples, as shown in Figure 13 (a) and (b). The temperature evolution curve can be divided into three main stages: the first stage is the heat storage process of the solid composite phase change material, the second stage is the phase change process from solid phase change material to liquid phase change material, and the third stage is the heat storage process of the liquid phase change material. The heat transfer process is essentially driven by the temperature gradient. As the heat storage process progresses, due to the gradually increasing temperature of SSPCMs, the temperature difference between HTF and SSPCMs keeps decreasing, thereby weakening the driving force of heat transfer. Therefore, the heating rate in the second stage is significantly lower than that in the first stage. In addition, the temperature rise curves of each monitoring point along the flow direction of HTF also show certain differences. Compared with monitoring point 1, the temperature rise curves of monitoring points 2, 3, 4, and 5 have a certain lag, and their temperatures are always lower than that of point 1. The temperature at 2-5 o'clock always decreases gradually as the altitude decreases. This phenomenon may be attributed to the heat exchange between the high-temperature HTF and the composite phase change material during its downward flow from the top: in the flow direction, the upper PCM first exchanges heat with HTF, and then the hot fluid continues to flow downward and exchanges heat with the middle and lower PCM. Due to the fact that the upper PCM has absorbed some heat, the HTF temperature decreases, thereby reducing the heat transfer driving force in the middle and lower regions, making their heat transfer efficiency relatively lower.

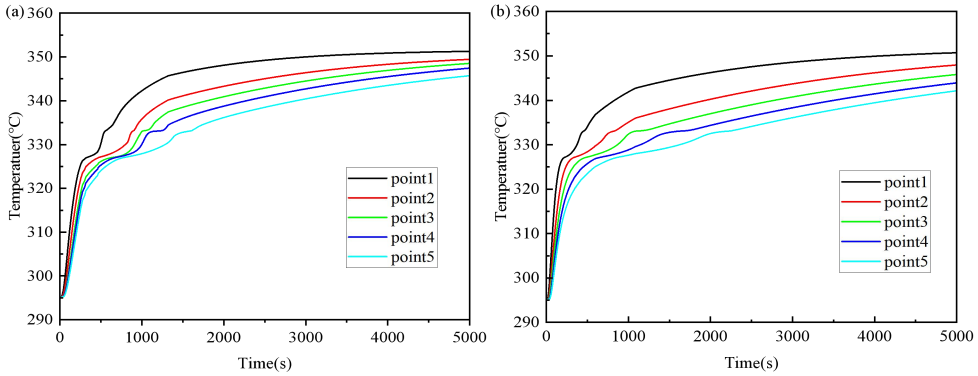

Figure 13. Temperature evolution history of selected points: points along HTF flow direction at (a) SSPCM-5 and (b) SSPCM-1.

Figure 14 shows the temperature distribution of SSPCM-1-SSPCM-5 at 1000 s, 2000 s, 3000 s and 4000 s. It clearly reveals the heat transfer process inside the energy storage latent heat device. It can be seen that the high-temperature area gradually expands over time. This phenomenon is characterized by heat first being transferred in the upper region, then spreading to the middle and lower regions. Meanwhile, the energy storage process of SSPCM-5 gradually approaches completion over time, and is basically fully charged at 2181 s. However, due to the convective heat transfer effect of the glass wall surface always present, as the system operation time increases, the temperature difference between the HTF and the wall surface gradually increases, thereby resulting in a corresponding enhancement of convective heat transfer intensity.

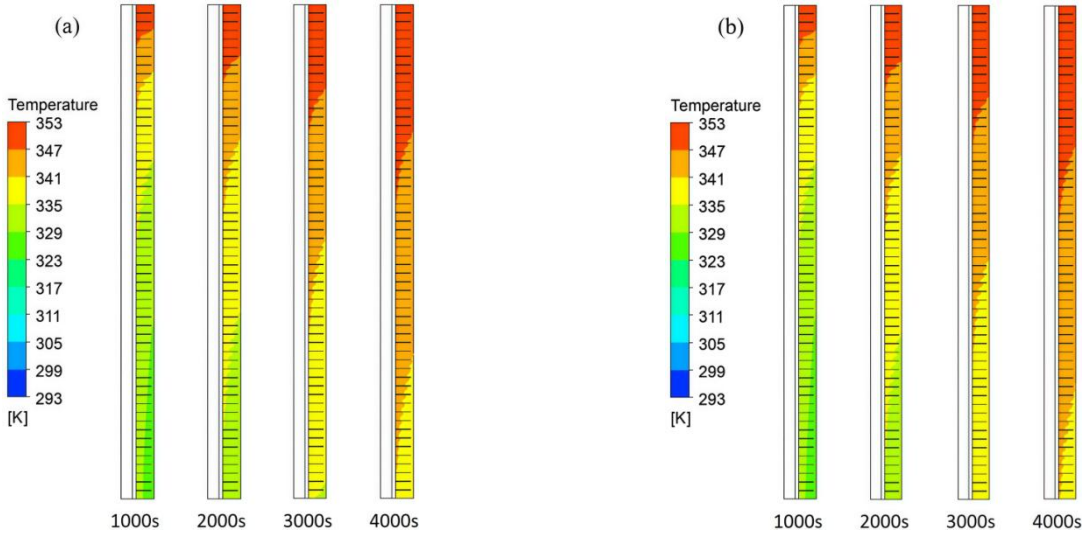

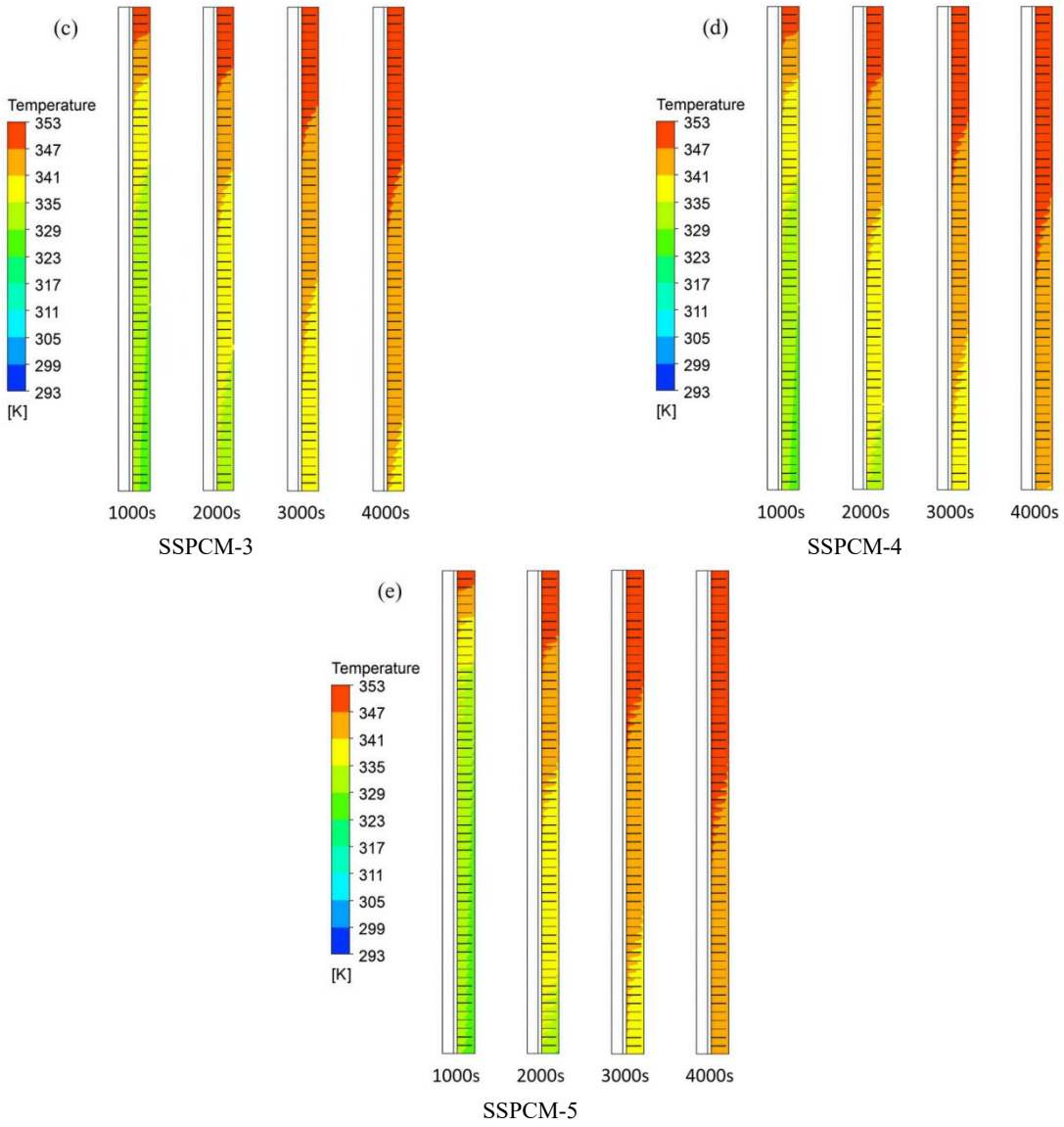

Figure 14. Temperature distribution contour maps of (a) SSPCM-1, (b) SSPCM-2, (c) SSPCM-3, (d) SSPCM-4 and (e) SSPCM-5 at 1000s, 2000s, 3000s, and 4000s.

To quantitatively characterize the heat storage process rate of SSPCM-1 to SSPCM-5, the thermal performance under the condition of enhanced heat conduction by the annular fins was evaluated using the temperature response rate (R(t)) during the charging process. The mathematical expression is as follows:

$$R(t) = \frac{T(t_i) - T(t_{i-1})}{\Delta t} \tag{13}$$

where $T(t_i)$ and $T(t_{i-1})$ represent the temperatures at time t_i and t_{i-1} respectively, and Δt represents the time interval between the two times. To evaluate the temperature response rate, the fixed monitoring point in SSPCMs was selected for analysis. Among the 5 fixed monitoring points, the temperature change trend of each material was the same. Taking point 3 as an example, the temperature changes of SSPCM-1 to SSPCM-5 are shown in Figure 15(a). It can be seen that the temperature change trends of the five composite materials are basically the same, among which SSPCM-5 reached the thermal stable state the earliest.

Since R(t) is a function of time, it cannot be directly used to quantify the heat transfer performance during the melting stage. Therefore, the integral average value of R(t) over the entire melting process is adopted for its quantitative evaluation.

$$\vec{R} = \frac{\int_0^{t_{fu}} R(t)dt}{t_{fu}} \tag{14}$$

where t_{fu} represents the complete melting time. It can be seen that the average response rate increases with the increase in the matrix content, and reaches its maximum in SSPCM-5. Recent studies mostly focused on fin structure optimization and single parameter analysis [42], lacking the combination of high-performance composite PCM and device simulation. This work combines material development with numerical simulation, proving that increasing MWCNT content can effectively shorten energy storage time and improve thermal response rate. The complete melting time of SSPCM-5 is significantly reduced compared with SSPCM-1, which provides a direct reference for material-device matching design in latent heat thermal energy storage systems.

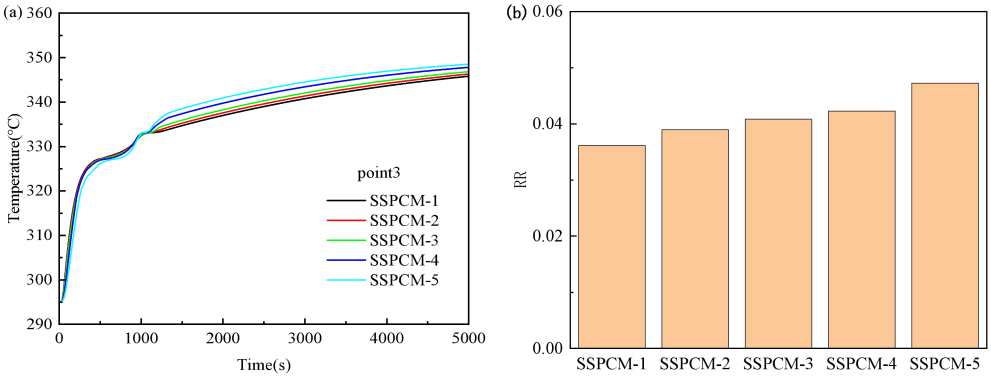

Figure 15. (a) Temperature evolution history of a given point (P3) for SSPCM-1-SSPCM-5; (b) response rate for finned LHTES with SSPCM-1-SSPCM-5.

4. Conclusion

This study used kaolin and MWCNT as the base materials and mixed them with PA to prepare SSPCMs. The modification effects of MWCNT and kaolin on the properties of PA were systematically investigated, and the leakage performance, chemical compatibility, and thermal physical properties (such as phase change temperature, phase change latent heat, and thermal conductivity, etc.) of SSPCM were analyzed. In addition, numerical simulation studies were conducted on the composite materials used in the latent heat energy storage device units. The main research results are as follows:

After introducing MWCNT into the PA-kaolin composite system, the structure of the composite material is more stable, and the microstructure changed significantly.

The addition of MWCNT can effectively improve the thermal conductivity of the material, and the chemical compatibility of the system remains good. When kaolin and 10% MWCNT are added together, the composite material has almost no leakage, and the melting point changes very little. Compared with pure PA, its thermal conductivity is increased by 4 times, the specific heat capacity and enthalpy value slightly decrease, and the energy storage density reaches 226.4 J/g, which is highly consistent with the theoretical enthalpy value and energy storage density.

Due to the excellent thermal stability and thermal conductivity of SSPCM, the energy storage process in the energy storage device is significantly accelerated, and the energy storage speed also increases with the increase in the content of the base material. In summary, SSPCM is a high-performance energy storage and thermal conductive composite material, and has broad application prospects in building energy conservation, industrial waste heat recovery, and environmental protection fields. Nevertheless, the present study still has certain limitations. The long-term thermal cycle stability and practical operational performance of the SSPCMs remain to be further verified and evaluated. In addition, simplified boundary conditions were employed in the numerical simulation process, and the complex variable operating conditions in actual engineering scenarios were not incorporated into the simulation model. Future research will focus on conducting systematic long-term cyclic performance tests and establishing more realistic numerical models that are consistent with practical operating conditions, thereby facilitating the extensive application of such composite phase change materials in actual engineering practices.

Acknowledgement: This work is supported by the National Natural Science Foundation of China (52576225, 52206274 and 52476085), Tianjin Education Commission Research Program Project (2023KJ206) and Natural Science Foundation of Tianjin (24JCQNJC00380).

Availability of Data and Materials: The datasets used and analyzed during the current study are available from the corresponding author on reasonable request.

Author Contributions: All authors contributed to the study conception and design, material preparation, data collection and analysis, and manuscript writing. All authors have read and approved the final manuscript. All authors contributed to editorial changes in the manuscript. All authors have participated sufficiently in the work and agreed to be accountable for all aspects of the work.

Conflict of Interest: The authors declare no conflict of interest.

References

1. Xu, J.; Zhang, X.; Zou, L. A review: Progress and perspectives of research on the functionalities of phase change materials. *Journal of Energy Storage* 2022, 54, 105341. https://doi.org/10.1016/j.est.2022.105341
2. Gayathri, R.; Shanmugha Soundare, S.; Mithren, M.; et al. Thermal and electrochemical analysis on SnSO3/ZnSO3 nanocomposite. *Journal of Ovonic Research* 2025, 21(2), 187-198. https://doi.org/10.15251/jor.2025.212.187
3. Waheed, Z.; Tahir, N.; El Aziz, K.A.; et al. Synthesis of sunlight responsive ternary G-C3N4/strontium ferrite/zeolite nanocomposite and investigation of its synergistic photocatalytic activity. *Journal of Ovonic Research* 2025, 21(6), 705-723. https://doi.org/10.15251/jor.2025.216.705
4. Knani, S.; Arshad, M.I.; Al-Buriahi, M.S.; et al. Development of chromium ion substituted Zn-Co-Ca-Fe-Ba ferrites for energy storage applications. *Journal of Ovonic Research* 2025, 21(4), 409-418. https://doi.org/10.15251/jor.2025.214.409
5. Javadi, F.S.; Metselaar, H.S.C.; Ganesan, P. Performance improvement of solar thermal systems integrated with phase change materials (PCM), a review. *Solar Energy* 2020, 206, 330-352. https://doi.org/10.1016/j.solener.2020.05.106

6. Farid, M.M.; Khudhair, A.M.; Razack, S.A.K.; et al. A review on phase change energy storage: materials and applications. *Energy Conversion and Management* 2004, 45(9-10), 1597-1615. https://doi.org/10.1016/j.enconman.2003.09.015
7. Huang, X.; Gao, X.; Xue, J.; et al. Comprehensive performance of building systems using sensible-latent heat composite energy storage structure under all-day solar radiation conditions. *Energy* 2025, 334, 137578. https://doi.org/10.1016/j.energy.2025.137578
8. Jiang, F.; Tao, M.; Cai, J.; et al. Modification of steel slag to prepare chlorides based composite phase change materials with shape stability for high-temperature thermal energy storage. *Chemical Engineering Journal* 2024, 491, 152062. https://doi.org/10.1016/j.cej.2024.152062
9. Man, X.; Lu, H.; Xu, Q.; et al. Review on the thermal property enhancement of inorganic salt hydrate phase change materials. *Journal of Energy Storage* 2023, 72, 108699. https://doi.org/10.1016/j.est.2023.108699
10. Jiang, L.; Zhao, L.; Zhang, R.; et al. Research of the thermal storage properties of thermally conductive carbon fiber-reinforced paraffin/olefin block copolymer composite phase change materials with thermotropic flexibility. *Journal of Energy Storage* 2024, 76, 109761. https://doi.org/10.1016/j.est.2023.109761
11. Wang, Y.; Wu, L.; Li, J. Experimental study of a paraffin-based composite phase change material with graphite sheet, copper powder and silver copper powder. *Case Studies in Thermal Engineering* 2024, 54, 104003. https://doi.org/10.1016/j.csite.2024.104003
12. Wang, T.; Wang, K.; Ye, F.; et al. Characterization and thermal properties of a shape-stable Na2CO3-K2CO3/coal fly ash/expanded graphite composite phase change materials for high-temperature thermal energy storage. *Journal of Energy Storage* 2021, 33, 102123. https://doi.org/10.1016/j.est.2020.102123
13. Li, C.; Li, Q.; Ge, R. Fabrication and investigation of paraffin based shape-stable composite phase change materials with styrene ethylene butylene styrene as supporting skeleton for low temperature thermal energy storage and management. *Journal of Energy Storage* 2023, 68, 107802. https://doi.org/10.1016/j.est.2023.107802
14. Chen, P.; Gao, X.; Wang, Y.; et al. Metal foam embedded in SEBS/paraffin/HDPE form-stable PCMs for thermal energy storage. *Solar Energy Materials and Solar Cells* 2016, 149, 60-65. https://doi.org/10.1016/j.solmat.2015.12.041
15. Qu, Y.; Wang, S.; Tian, Y.; et al. Comprehensive evaluation of Paraffin-HDPE shape stabilized PCM with hybrid carbon nano-additives. *Applied Thermal Engineering* 2019, 163, 114404. https://doi.org/10.1016/j.applthermaleng.2019.114404
16. Zhang, Y.; Zheng, S.; Zhu, S.; et al. Evaluation of paraffin infiltrated in various porous silica matrices as shape-stabilized phase change materials for thermal energy storage. *Energy Conversion and Management* 2018, 171, 361-370. https://doi.org/10.1016/j.enconman.2018.06.002
17. Mekaddem, N.; Ali, S.B.; Fois, M.; et al. Paraffin/ Expanded Perlite/Plaster as Thermal Energy Storage Composite. *Energy Procedia* 2019, 157, 1118-1129. https://doi.org/10.1016/j.egypro.2018.11.279
18. Hu, C.; Jiang, Y.; Chen, S.; et al. Copper foam reinforced polymer-based phase change material composites for more efficient thermal management of lithium-ion batteries. *Journal of Energy Storage* 2023, 73, 108918. https://doi.org/10.1016/j.est.2023.108918
19. Atinafu, D.G.; Yun, B.Y.; Wi, S.; et al. A comparative analysis of biochar, activated carbon, expanded graphite, and multi-walled carbon nanotubes with respect to PCM loading and energy-storage capacities. *Environmental Research* 2021, 195, 110853. https://doi.org/10.1016/j.envres.2021.110853
20. Hekimoğlu, G.; Sarı, A.; Gencel, O.; et al. Activated carbon/expanded graphite hybrid structure for development of nonadecane based composite PCM with excellent shape stability, enhanced thermal

conductivity and heat charging-discharging performance. *Thermal Science and Engineering Progress* 2023, 44, 102081. https://doi.org/10.1016/j.tsep.2023.102081

21. Zhou, D.; Zhao, C.Y. Experimental investigations on heat transfer in phase change materials (PCMs) embedded in porous materials. *Applied Thermal Engineering* 2011, 31, 970-977. https://doi.org/10.1016/j.applthermaleng.2010.11.022
22. V, J.; S, G.; N, B.; et al. Experimental investigation of cascaded thermal energy storage systems using finned encapsulated phase change materials. *Results in Engineering* 2025, 25, 104395. https://doi.org/10.1016/j.rineng.2025.104395
23. Ben-Ali, S.; Nouri, H.; Mekaddem, N.; et al. Bio-based pomegranate peel/paraffin wax phase change composites for enhanced thermal energy storage. *Results in Engineering* 2025, 27, 106317. https://doi.org/10.1016/j.rineng.2025.106317
24. Wang, S.; Lei, K.; Wang, Z.; et al. Metal-based phase change material (PCM) microcapsules/nanocapsules: Fabrication, thermophysical characterization and application. *Chemical Engineering Journal* 2022, 438, 135559. https://doi.org/10.1016/j.cej.2022.135559
25. Soni, K.; Panwar, N.L. Revolutionizing thermal energy storage: An overview of porous support materials for advanced composite Phase Change Materials (PCMs). *Progress in Engineering Science* 2024, 1, 100023. https://doi.org/10.1016/j.pes.2024.100023
26. Cao, X.; Li, C.; He, G.; et al. Composite phase change materials of ultra-high molecular weight polyethylene/paraffin wax/carbon nanotubes with high performance and excellent shape stability for energy storage. *Journal of Energy Storage* 2021, 44, 103460. https://doi.org/10.1016/j.est.2021.103460
27. Kanti, P.K.; Wanatasanappan, V.V.; Said, N.M.; et al. Application of predictive models and thermal enhancement of phase change material with multi walled carbon nanotubes–Al_2O_3 hybrid nanoparticles. *Journal of Energy Storage* 2026, 152, 120665. https://doi.org/10.1016/j.est.2026.120665
28. Ren, F.; Hou, J.; Shi, C.; et al. Hydrophilicity regulation of carbon nanotubes as phase-change materials for thermal energy storage. *Journal of Materials Research and Technology* 2024, 30, 1482-1489. https://doi.org/10.1016/j.jmrt.2024.03.173
29. Karaipekli, A.; Biçer, A.; Sarı, A.; et al. Thermal characteristics of expanded perlite/paraffin composite phase change material with enhanced thermal conductivity using carbon nanotubes. *Energy Conversion and Management* 2017, 134, 373-381. https://doi.org/10.1016/j.enconman.2016.12.053
30. Subasi, A.; Subasi, S.; Bayram, M.; et al. Effect of carbon nanotube and microencapsulated phase change material utilization on the thermal energy storage performance in UV cured (photoinitiated) unsaturated polyester composites. *Journal of Energy Storage* 2023, 61, 106780. https://doi.org/10.1016/j.est.2023.106780
31. Lv, P.; Liu, C.; Rao, Z. Experiment study on the thermal properties of paraffin/kaolin thermal energy storage form-stable phase change materials. *Applied Energy* 2016, 182, 475-487. https://doi.org/10.1016/j.apenergy.2016.08.147
32. Grzywacz, H.; Jarząbek, D.M.; Pietrzyk-Thel, P.; et al. Low-content MWCNTs–PVDF composites for nanoscale actuation: Crystalline tailoring and in-situ electro-mechanical analysis using hybrid AFM–Sawyer-Tower system. *Carbon* 2025, 245, 120738. https://doi.org/10.1016/j.carbon.2025.120738
33. Lu, Z.; Xu, B.; Zhang, J.; et al. Preparation and characterization of expanded perlite/paraffin composite as form-stable phase change material. *Solar Energy* 2014, 108, 460-466. https://doi.org/10.1016/j.solener.2014.08.008
34. Liu, S.; Yang, H. Stearic acid hybridizing coal–series kaolin composite phase change material for thermal energy storage. *Applied Clay Science* 2014, 101, 277-281. https://doi.org/10.1016/j.clay.2014.09.002

35. Shen, Z.; Kwon, S.; Lee, H.L.; et al. Cellulose nanofibril/carbon nanotube composite foam-stabilized paraffin phase change material for thermal energy storage and conversion. *Carbohydrate Polymers* 2021, 273, 118585. https://doi.org/10.1016/j.carbpol.2021.118585
36. Qi, R.; Pan, T.; Guo, Z.; et al. Enhancement properties of lamellar porous copper/paraffin composite materials by freeze casting. *Journal of Energy Storage* 2025, 132, 117873. https://doi.org/10.1016/j.est.2025.117873
37. Dananjaya, V.; Bao, X.; Hansika, N.; et al. Structural and thermal properties of paraffin-based graphene and carbon fibre composite phase change materials. International *Journal of Heat and Mass Transfer* 2026, 255, 127696. https://doi.org/10.1016/j.ijheatmasstransfer.2025.127696
38. Fan, L.-W.; Fang, X.; Wang, X.; et al. Effects of various carbon nanofillers on the thermal conductivity and energy storage properties of paraffin-based nanocomposite phase change materials. *Applied Energy* 2013, 110, 163-172. https://doi.org/10.1016/j.apenergy.2013.04.043
39. Xiong, S.; Shi, Y.; Liu, C.; et al. A photothermal energy storage phase change material with high stability and enthalpy††Electronic supplementary information (ESI) available. *RSC Advances* 2025, 15(21), 17023-17030. https://doi.org/10.1039/d5ra01422k
40. Yang, X.; Lu, Z.; Bai, Q.; et al. Thermal performance of a shell-and-tube latent heat thermal energy storage unit: Role of annular fins. *Applied Energy* 2017, 202, 558-570. https://doi.org/10.1016/j.apenergy.2017.05.007
41. Longeon, M.; Soupart, A.; Fourmigué, J.-F.; et al. Experimental and numerical study of annular PCM storage in the presence of natural convection. *Applied Energy* 2013, 112, 175-184. https://doi.org/10.1016/j.apenergy.2013.06.007
42. Ye, W.; Khodadadi, J.M. Effects of varying geometrical parameters on the melting performance of phase change materials within L-shaped shell-and-tube latent heat thermal energy storage units with radial eccentricity exhibiting prominent influence. *Journal of Energy Storage* 2024, 86, 111334. https://doi.org/10.1016/j.est.2024.111334